Star-shaped oscillations of Leidenfrost drops

Xiaolei Ma,[*] Juan-José Liétor-Santos, and Justin C. Burton

Department of Physics, Emory University, Atlanta, Georgia 30322, USA

We experimentally investigate the self-sustained, star-shaped oscillations of Leidenfrost drops. The drops levitate on a cushion of evaporated vapor over a heated, curved surface. We observe modes with $n = 2$–13 lobes around the drop periphery. We find that the wavelength of the oscillations depends only on the capillary length of the liquid and is independent of the drop radius and substrate temperature. However, the number of observed modes depends sensitively on the liquid viscosity. The dominant frequency of pressure variations in the vapor layer is approximately twice the drop oscillation frequency, consistent with a parametric forcing mechanism. Our results show that the star-shaped oscillations are driven by capillary waves of a characteristic wavelength beneath the drop and that the waves are generated by a large shear stress at the liquid-vapor interface.

The Leidenfrost effect can be easily observed by placing a millimeter-scale water drop onto a sufficiently hot pan. The drop will levitate on a thermally insulating vapor layer and survive for minutes [1–4]. The complex interactions between the liquid, vapor, and solid interfaces have led to a broad range of applications such as turbulent drag reduction [5], self-propulsion of drops on ratcheted surfaces [6,7], green nanofabrication [8], fuel combustion [9], and thermal control of nuclear reactors [10]. Given the importance of the Leidenfrost effect for both friction reduction and thermal insulation, we know surprisingly little about the detailed coupling between the liquid and the thin vapor layer.

This coupling can be probed by investigating the dynamics of drop oscillations. Leidenfrost drops experience both small- and large-amplitude oscillations with very little damping. For small drops, the geometry of the vapor layer and resulting drop dynamics have recently been characterized [11,12]. Large Leidenfrost drops are well known to form self-sustained, star-shaped oscillations [Fig. 1(a)]. Since the 1950s, a number of studies have investigated these star oscillations, often with different conclusions as to their physical origin due to the complicated interplay between thermal and hydrodynamic effects in both the liquid and gas phases [13–19]. The underlying mechanism for the onset of star oscillations remains unknown.

Here we report measurements of star-shaped oscillations of six different liquids on a hot, curved surface. We observe stars with $n = 2$–13 lobes around the drop periphery. Although the number of observed modes depends on the liquid viscosity and substrate temperature, we find that the wavelength and frequency of the modes depend only on the capillary length, $l_c = \sqrt{\gamma / \rho_l g}$, where γ and ρ_l are the surface tension and density of the liquid and g is gravitational acceleration. The pressure near the center of the vapor layer oscillates at approximately twice the frequency of the drop oscillation, consistent with a parametric coupling mechanism. We show that this pressure variation stems from capillary waves of a characteristic wavelength, $\lambda_c \approx 4l_c$, generated by a large shear stress at the liquid-vapor interface beneath the drop.

In the experiment, most substrates were constructed from blocks of engineering 6061 aluminum alloy with dimensions $7.6 \times 7.6 \times 2.5$ cm. The substrate temperature was controlled by resistive heaters embedded in the material. Six different liquids were used as Leidenfrost drops: deionized water, liquid N_2, acetone, methanol, ethanol, and isopropanol. The physical properties of each liquid
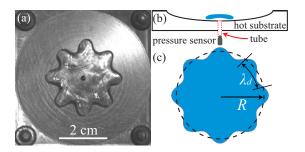
---

[*]xiaolei.ma@emory.edu

FIG. 1. (a) Top-down image of a star-shaped Leidenfrost water drop ($l_c = 2.5$ mm, $R = 1.4$ cm, $T_s = 623$ K). The small, dark circle in the center of the substrate is used for pressure measurements. (b) Cross-sectional view of the experimental setup. (c) Top-down schematic of a star-shaped drop indicating the radius R and wavelength $\lambda_d = 2\pi R/n$.

at the boiling point T_b are listed in Table I. For water, the substrate temperature T_s varied from 493 to 773 K, while for ethanol, methanol, acetone, and isopropanol, T_s was set to 523 K. The substrate for liquid N_2 was not heated due to its extremely low T_b. Movies of water drop oscillations corresponding to modes $n = 2, 4, 8$, and 11 can be found in the Supplemental Material (Movies S1–S4) [20].

The upper surfaces of the substrates were machined into a spherical bowl shape in order to suppress the buoyancy-driven Rayleigh-Taylor instability in the vapor layer and keep the drops stationary [4,21,22]. A cross-sectional view of the curved substrates is shown in Fig. 1(b). The curvature of each surface was designed to satisfy $l_c/R_s = 0.03$, where R_s is the radius of curvature of the surface. For some experiments, a plano-concave, fused silica lens (focal length = 250 mm) was used as the heated substrate in order to allow for optical imaging of the vapor layer beneath the oscillating drop.

We used a high-speed digital camera (Phantom V7.11, Vision Research) with a resolution of 132 pixels/cm to image the drops at 1000 frames/s. Recorded videos were then analyzed to obtain the frequency and wavelength of the star-shaped oscillations. An image of a water drop (mode $n = 8$) is shown in Fig. 1(a) (Movie S3) [20]. A schematic of a typical star-shaped oscillation mode is shown in Fig. 1(c), indicating the radius R and wavelength of the standing wave λ_d. In order to detect pressure variations beneath the drop, a pressure sensor (GEMS Sensors, response time of 5 ms, sensitivity of 2 mV/Pa) was connected to a small hole with a diameter of 1 mm at the center of the curved aluminum [Fig. 1(a)]. The pressure was sampled at 500–1000 Hz in order to accurately capture waveforms near the response time of the sensor.

For each observed star-shaped oscillation mode, we measured the azimuthal wavelength λ_d, drop oscillation frequency f_d, and the characteristic frequency of pressure oscillations f_p. Figure 2(a) shows the excess pressure (above atmosphere) before the initiation of a star-shaped oscillation for a

TABLE I. Physical properties of different liquids at the boiling point T_b (K). Units are as follows: γ, mN/m; ρ_l, kg/m^3; η_l, mPa s; l_c (mm). Data were taken from Ref. [23].

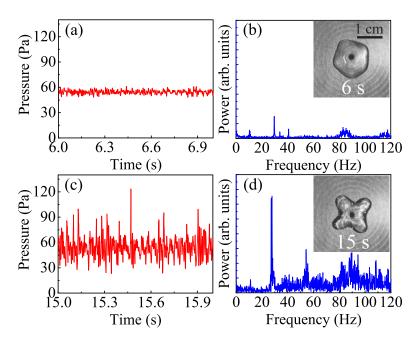| Liquid	T_b	γ	ρ_l	η_l	l_c	Mode	Re_l
Water	373	59.0	958	0.282	2.5	2–13	1340
Liquid N_2	77	8.90	807	0.162	1.1	3–5, 7	539
Acetone	329	18.2	727	0.242	1.6	5–10	601
Methanol	338	18.9	748	0.295	1.6	6–10	511
Ethanol	352	18.6	750	0.420	1.6	7–11	355
Isopropanol	356	15.7	723	0.460	1.5	9, 10	283

FIG. 2. (a) Pressure variations in the vapor layer beneath a Leidenfrost water drop ($T_s = 623$ K) just before the initiation of the star-shaped oscillation. (b) Power spectrum of the pressure fluctuations over the time interval of 0–9 s. (c) Pressure variations during a fully developed $n = 4$ mode. (d) Power spectrum of the pressure fluctuations over the time interval of 9–18 s, showing a sharp peak at $f_p \approx 28$ Hz. Both power spectra have the same linear vertical scale. The insets in (b) and (d) show snapshots of the drop shape, and the scale bar of 1 cm applies to both images.

water drop. For a very large drop, i.e., $R \gg l_c$, the drop can be approximated by a cylinder whose thickness, $h \approx 2l_c$, is determined by a balance of surface tension and gravitational forces [2]. Thus the mean pressure required to levitate a large Leidenfrost water drop at the boiling point should be $\rho_l g h \approx 47$ Pa. One can see that the pressure measured in the center is slightly larger than 47 Pa. This is expected since a radial pressure gradient is required to drive the viscous vapor from the center of the drop to the edge.

Figure 2(b) shows the Fourier power spectrum of the pressure prior to the initiation of a star oscillation. There is a visible peak at $f_p \approx 30$ Hz, as well as small peaks at higher frequencies. Figure 2(c) shows data for the same drop later in time during a well-developed $n = 4$ mode oscillation (Movie S2) [20]. Large variations in the pressure are visible, although the mean pressure remains unchanged. Figure 2(d) shows the power spectrum during the star-shaped oscillation, indicating a sharp peak at $f_p \approx 28$ Hz, in addition to noise and harmonics at higher frequencies. The star-shaped oscillation frequency for this drop was $f_d \approx 14$ Hz $\approx f_p/2$.

To gain further insight into the origin of the star-shaped oscillations, we used five other liquids in addition to water, as listed in Table I. A summary of our results is shown in Fig. 3. The error bars of R, λ_d, and f_d come from the standard deviation of multiple measurements from different drops, whereas the error bar of f_p is taken from the full width of the highest peak in the power spectrum at half the maximum value, as shown in Fig. 2(d). For all the liquids, $f_d \approx f_p/2$, in agreement with a parametric forcing mechanism [24,25]. The data collapse very well when scaled only by l_c and the frequency scale $(g/l_c)^{1/2}$. This collapse works for all the liquids used in the experiments, as well as water drops at different substrate temperatures, suggesting a purely hydrodynamic (nonthermal) mechanism for generating star-shaped oscillations. This is in agreement with recent experiments studying star-shaped oscillations of drops levitated by an air flow from below [26].
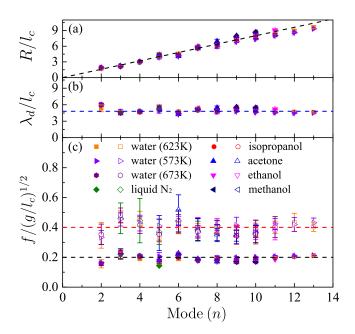
FIG. 3. (a) Normalized radius, (b) wavelength, and (c) frequency versus oscillation mode number n. Frequencies are plotted for both the star-shaped drop (f_d, solid symbols) and vapor layer pressure oscillations (f_p, open symbols). The error bars are described in the main text. The dashed line in (a) is the best linear fit to the data, whereas the dashed lines in (b) and (c) represent the mean values of the data.

Since λ_d is approximately constant, modes with large n could be observed only in large drops. Occasionally, we observed the same mode number at smaller values of R, but this happened only for $n = 2$–4 and was difficult to replicate. In addition, we found that the number of observed modes was sensitive to the viscosity of the liquid. Assuming a characteristic length l_c and time scale $\sqrt{l_c^3 \rho_l / \gamma}$, we express the Reynolds number associated with the flow of each liquid, $\mathrm{Re}_l \equiv (l_c \gamma \rho_l)^{1/2} / \eta_l$, as shown in Table I. We find that the minimum observed mode number n_{min} is inversely proportional to Re_l, as shown in Fig. 4. This suggests that liquid viscosity damps the oscillations of smaller drops and thus sets the threshold mode for self-sustained star oscillations. The largest observable value of n is ultimately determined by the size of the experimental apparatus, except in the case of liquid N_2, where the evaporation rate is very high since the substrate temperature is much higher than the boiling point. Even though the substrate is curved, for large drops the resulting vapor layer is thick enough to develop bubbles due to the Rayleigh-Taylor instability [21].
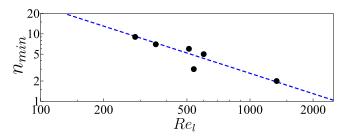

FIG. 4. Scaling behavior for the minimum observed star mode n_{min} with respect to Re_l of different liquids (Table I). The blue dashed line represents $2600\,\mathrm{Re}_l^{-1}$.
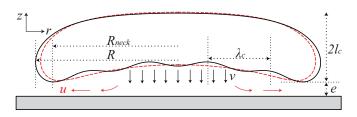
FIG. 5. Cartoon cross section of a Leidenfrost drop before (red dashed curve) and after (black curve) the excitation of capillary waves under the drop. Symbols are defined in the text.

One surprising result drawn from the experimental data is that only a single dominant wavelength (and thus frequency) exists for all modes and depends only on l_c. There are small oscillations of both λ_d and f_d about their mean values [dashed lines in Figs. 3(b) and 3(c)]. These oscillations are strongest for small n and are consistent among the different liquids and substrate temperatures. This phenomenon may be caused by nonlinear effects; for example, the dependence of the oscillation frequency on the amplitude is stronger for smaller modes [27,28]. Nevertheless, the data suggest a very robust mechanism for selecting either the frequency or wavelength of the modes.

The relationship between f_d and f_p can be understood from the quasi-two-dimensional dispersion relation for large, puddle-shaped drops, where $f_d \propto R^{-3/2}$ [26,29,30]. Assuming that the radius of the puddle varies sinusoidally with time, modes of the star oscillations follow an equation similar to the Mathieu equation and will be excited when $f_d \approx f_p/2$ [24,29]. In the case of Leidenfrost drops, there is no obvious frequency or wavelength selection mechanism generated by the flow and evaporation of vapor beneath the drop. It is possible that a "breathing mode" of the drop would cause the radius to vary with time; however, recent measurements of the breathing mode in both low- and high-viscosity levitated drops show that the frequency rapidly decreases with R [12,26,31], in contrast to the data shown in Fig. 3(c).

The pressure variations beneath the drop are determined by the shape of the liquid-vapor interface and the flow in the vapor layer. A simple model of the flow beneath the drop is shown in Fig. 5, where v is the velocity of the gas at the liquid surface, e is the mean thickness of the vapor layer, and u is the radial velocity of the gas near $r = R$. Following the model in Biance $et\ al.$ [2] by assuming incompressibility and lubrication flow in the gas, e, v, and u can be expressed as

$$u = \left(\frac{\rho_l g \kappa l_c}{3 \rho_v \eta_v L} \right)^{1/2} \Delta T^{1/2}, \tag{1}$$

$$v = \left[\frac{4 l_c \rho_l g}{3 \eta_v} \left(\frac{\kappa \Delta T}{L \rho_v} \right)^3 \right]^{1/4} R^{-1/2}, \tag{2}$$

$$e = \left(\frac{3 \kappa \Delta T \eta_v}{4 L \rho_l \rho_v g l_c} \right)^{1/4} R^{1/2}, \tag{3}$$

where $\Delta T = T_s - T_b$, L is the latent heat of evaporation, and η_v, ρ_v, and κ are the mean values of the dynamic viscosity, density, and thermal conductivity in the vapor layer, respectively. Although the approximation assumes a steady-state, linear temperature profile in the vapor layer, this is valid since the typical thermal diffusion time across the vapor layer is ≈ 1 ms for water vapor near the boiling point.

The Reynolds number in the vapor layer can be expressed as $\mathrm{Re}_v \equiv v e \rho_v / \eta_v$ [32,33]. After plugging in the expressions for v and e, $\mathrm{Re}_v = \Delta T \kappa / L \eta_v$, which is independent of the drop radius. For typical values of the properties in a water vapor layer, $\mathrm{Re}_v \approx 0.2$. Thus both viscous and inertial
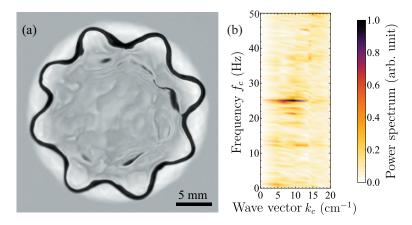
FIG. 6. (a) Capillary waves imaged beneath an $n = 8$ mode acetone drop. The image has been enhanced for visibility. (b) Corresponding power spectrum associated with the acetone Leidenfrost drop. There is a sharp peak at $f_c \approx 26$ Hz which covers a broad range of wave vectors.

forces are relevant. However, a simple estimate of the Bernoulli pressure, $\rho_v u^2/2 \approx 1$ Pa, suggests that inertia is not responsible for the pressure variations observed in Fig. 2.

On the other hand, the viscous lubrication pressure scales as $\eta_v v R^2/e^3$, so that variations in pressure are related to small thickness changes: $\Delta p = (3\eta_v v R^2/e^4)\Delta e$. For the water drop shown in Fig. 2(d), where $\Delta p \approx 10$ Pa, we would expect thickness variations of order $\Delta e \approx 15$ μm. These variations could be produced by a vertical motion of the center of mass of the drop, although the frequency of this oscillation should decrease for larger drops, in contrast to the data in Fig. 3(c). Thus it is likely that the pressure oscillations occur due to local changes in vapor thickness.

We hypothesize that the pressure variations are caused by capillary waves of a characteristic wavelength (frequency) λ_c (f_c) which travel from the center of the drop to the edge. When they reach the edge, the waves will cause the radius to vary with time, as shown schematically in Fig. 5. To support this hypothesis, we have measured the spectrum of capillary waves by imaging the vapor layer under a star-shaped Leidenfrost drop on a curved, fused silica surface. Variations in the thickness of the vapor layer deflect the collimated light used for illumination. A typical image under an acetone drop is shown in Fig. 6(a), and the corresponding power spectrum is shown in Fig. 6(b). The spectrum shows a large peak at $f_c \approx 26$ Hz which is spread over a range of wave numbers located near $k_c \approx 10$ cm^{-1}.

The exact selection mechanism for the dominant wavelength λ_c beneath the drop is the result of interactions between the lubricating flow of the evaporating vapor and the deformable liquid interface. Capillary waves with small wavelengths are known to be unstable when a liquid interface is driven by a strong shear stress [34–37]. For water waves, the strength of the shear is often measured by the friction velocity, $u_\star = \sqrt{\tau/\rho_v}$, where τ is the shear stress at the interface. Assuming a parabolic-flow profile in the vapor layer with mean velocity u near the edge of the drop (Fig. 5), the maximum shear stress at the liquid-vapor interface is $\tau = 6\eta_v u/e$. Plugging in the expressions for u and e from Eqs. (1) and (3) and using typical values for the properties of water vapor, we estimate that $u_\star \approx 1$–2 m/s for a Leidenfrost drop. This friction velocity is quite strong and can easily lead to the unstable growth of modes with wavelengths of the order of a few millimeters [35,36]. The threshold for the onset of instability, as shown in Fig. 4, should also be related to the forcing and velocity in the vapor layer [26]. This remains an open question for future studies.

We can estimate for the dominant wave vector using the zeroth-order dispersion relation for capillary waves under the drop. We assume a constant pressure in the vapor layer and that the top

surface of the drop is nearly flat:

$$f_c = \frac{1}{2\pi} \sqrt{\left(-g k_c + \frac{\gamma k_c^3}{\rho_l}\right) \tanh(k_c h)}. \tag{4}$$

Here $k_c = 2\pi/\lambda_c$, and $h \approx 2l_c$ is the thickness of the drop. This is the well-known dispersion relation for capillary-gravity waves, except the denser fluid rests above the lighter gas. Since we are not considering the restoring force associated with the lubrication pressure, our estimate serves as an upper bound for k_c. For a large Leidenfrost water drop, the measured frequency of pressure variations is $f_p \approx 26$ Hz. Using Eq. (4) and assuming $f_p = f_c$, we arrive at $\lambda_c \approx 3.03 l_c$. For the acetone drop shown in Fig. 6(a), this corresponds to $k_c \approx 12.9$ cm^{-1}, which is slightly larger than the position of the peak in Fig. 6(b).

This result is also in agreement with the minimum value of R required to observe an $n = 2$ mode (Movie S1) [20]. The drop radius we measured is the maximum radius R instead of R_{neck}, which is the radius at which the drop comes closest to the substrate (Fig. 5). The minimum size necessary to fit one wavelength beneath the drop is $R_{\text{neck}} = \lambda_c/2$. The relationship between R and R_{neck} for large Leidenfrost drops is $R \approx R_{\text{neck}} + 0.53 l_c$ [11,22]. This means that the minimum value of R required to observe a star-shaped oscillation is $R \approx 2.05 l_c$, in agreement with data shown in Fig. 3(a).

In summary, the dynamics of the vapor layer under a star-shaped Leidenfrost drop involve a rich spectrum of physical processes, including multiphase heat and mass transfer, interfacial wave generation, lubricating flow, and self-sustained parametric oscillations. Given this complexity, surprisingly, the star oscillation wavelength and frequency are nearly independent of the drop radius, mode number, and substrate temperature and depend only on the capillary length of the liquid, indicating a purely hydrodynamic (nonthermal) origin for the oscillations. We demonstrate that capillary waves of a characteristic wavelength beneath the drop lead to pressure oscillations in the vapor layer, which parametrically induce the star-shaped oscillations. These results may enhance our understanding of thin, supporting gas films in contact with a liquid interface and a solid surface, a scenario which occurs during drop impact and gas entrainment.

---

[1] J. G. Leidenfrost, *De Aquae Communis Nonnullis Qualitatibus Tractatus* (Ovenius, Duisburg, 1756).

[2] A.-L. Biance, C. Clanet, and D. Quéré, Leidenfrost drops, Phys. Fluids **15**, 1632 (2003).

[3] B. S. Gottfried and K. J. Bell, Film boiling of spheroidal droplets. Leidenfrost phenomenon, Ind. Eng. Chem. Fundam. **5**, 561 (1966).

[4] D. Quéré, Leidenfrost dynamics, Annu. Rev. Fluid Mech. **45**, 197 (2013).

[5] I. U. Vakarelski, J. O. Marston, D. Y. C. Chan, and S. T. Thoroddsen, Drag Reduction by Leidenfrost Vapor Layers, Phys. Rev. Lett. **106**, 214501 (2011).

[6] H. Linke, B. J. Alemán, L. D. Melling, M. J. Taormina, M. J. Francis, C. C. Dow-Hygelund, V. Narayanan, R. P. Taylor, and A. Stout, Self-Propelled Leidenfrost Droplets, Phys. Rev. Lett. **96**, 154502 (2006).

[7] G. Lagubeau, M. Le Merrer, C. Clanet, and D. Quéré, Leidenfrost on a ratchet, Nat. Phys. **7**, 395 (2011).

[8] R. Abdelaziz, D. Disci-Zayed, M. K. Hedayati, J.-H. Pöhls, A. U. Zillohu, B. Erkartal, V. S. K. Chakravadhanula, V. Duppel, L. Kienle, and M. Elbahri, Green chemistry and nanofabrication in a levitated Leidenfrost drop, Nat. Commun. **4**, 2400 (2013).

[9] T. Kadota, H. Tanaka, D. Segawa, S. Nakaya, and H. Yamasaki, Microexplosion of an emulsion droplet during Leidenfrost burning, Proc. Combust. Inst. **31**, 2125 (2007).

[10] H. Van Dam, Physics of nuclear reactor safety, Rep. Prog. Phys. **55**, 2025 (1992).

[11] J. C. Burton, A. L. Sharpe, R. C. A. van der Veen, A. Franco, and S. R. Nagel, Geometry of the Vapor Layer Under a Leidenfrost Drop, Phys. Rev. Lett. **109**, 074301 (2012).

[12] T. A. Caswell, Dynamics of the vapor layer below a Leidenfrost drop, Phys. Rev. E **90**, 013014 (2014).

[13] N. J. Holter and W. R. Glasscock, Vibrations of evaporating liquid drops, J. Acoust. Soc. Am. **24**, 682 (1952).

[14] D. E. Strier, A. A. Duarte, H. Ferrari, and G. B. Mindlin, Nitrogen stars: Morphogenesis of a liquid drop, Phys. A (Amsterdam, Neth.) **283**, 261 (2000).

[15] N. Tokugawa and R. Takaki, Mechanism of self-induced vibration of a liquid drop based on the surface tension fluctuation, J. Phys. Soc. Jpn. **63**, 1758 (1994).

[16] K. Adachi and R. Takaki, Vibration of a flattened drop. I. Observation, J. Phys. Soc. Jpn. **53**, 4184 (1984).

[17] R. Takaki and K. Adachi, Vibration of a flattened drop. II. Normal mode analysis, J. Phys. Soc. Jpn. **54**, 2462 (1985).

[18] F. Celestini, T. Frisch, A. Cohen, C. Raufaste, L. Duchemin, and Y. Pomeau, Two dimensional Leidenfrost droplets in a Hele-Shaw cell, Phys. Fluids **26**, 032103 (2014).

[19] A. Snezhko, E. B. Jacob, and I. S. Aranson, Pulsating–gliding transition in the dynamics of levitating liquid nitrogen droplets, New J. Phys. **10**, 043034 (2008).

[20] See Supplemental Material at http://link.aps.org/supplemental/10.1103/PhysRevFluids.2.031602 for movies of water drop oscillations corresponding to modes $n = 2, 4, 8$, and 11.

[21] P. H. Trinh, H. Kim, N. Hammoud, P. D. Howell, S. J. Chapman, and H. A. Stone, Curvature suppresses the Rayleigh-Taylor instability, Phys. Fluids **26**, 051704 (2014).

[22] J. H. Snoeijer, P. Brunet, and J. Eggers, Maximum size of drops levitated by an air cushion, Phys. Rev. E **79**, 036307 (2009).

[23] E. W. Lemmon, M. O. McLinden, D. G. Friend, P. J. Linstrom, and W. G. Mallard, *NIST Chemistry WebBook*, NIST Standard Reference Database Vol. 69 (NIST, Gaithersburg, MD, 2011).

[24] P. Brunet and J. H. Snoeijer, Star-drops formed by periodic excitation and on an air cushion—A short review, Eur. Phys. J. Spec. Top. **192**, 207 (2011).

[25] C. L. Shen, W. J. Xie, and B. Wei, Parametrically excited sectorial oscillation of liquid drops floating in ultrasound, Phys. Rev. E **81**, 046305 (2010).

[26] W. Bouwhuis, K. G. Winkels, I. R. Peters, P. Brunet, D. van der Meer, and J. H. Snoeijer, Oscillating and star-shaped drops levitated by an airflow, Phys. Rev. E **88**, 023017 (2013).

[27] E. Becker, W. J. Hiller, and T. A. Kowalewski, Experimental and theoretical investigation of large-amplitude oscillations of liquid droplets, J. Fluid Mech. **231**, 189 (1991).

[28] W. R. Smith, Modulation equations for strongly nonlinear oscillations of an incompressible viscous drop, J. Fluid Mech. **654**, 141 (2010).

[29] N. Yoshiyasu, K. Matsuda, and R. Takaki, Self-induced vibration of a water drop placed on an oscillating plate, J. Phys. Soc. Jpn. **65**, 2068 (1996).

[30] X. Ma, J.-J. Liétor-Santos, and J. C. Burton, The many faces of a Leidenfrost drop, Phys. Fluids **27**, 091109 (2015).

[31] X. Ma, J.-J. Liétor-Santos, and J. C. Burton, Dynamics of self-organized oscillations of Leidenfrost drops (unpublished).

[32] J. R. Lister, A. B. Thompson, A. Perriot, and L. Duchemin, Shape and stability of axisymmetric levitated viscous drops, J. Fluid Mech. **617**, 167 (2008).

[33] L. Duchemin, J. R. Lister, and U. Lange, Static shapes of levitated viscous drops, J. Fluid Mech. **533**, 161 (2005).

[34] J. W. Miles, On the generation of surface waves by shear flows, J. Fluid Mech. **3**, 185 (1957).

[35] X. Zhang, Capillary-gravity and capillary waves generated in a wind wave tank: Observations and theories, J. Fluid Mech. **289**, 51 (1995).

[36] A. Zeisel, M. Stiassnie, and Y. Agnon, Viscous effects on wave generation by strong winds, J. Fluid Mech. **597**, 343 (2008).

[37] A. Paquier, F. Moisy, and M. Rabaud, Surface deformations and wave generation by wind blowing over a viscous liquid, Phys. Fluids **27**, 122103 (2015).